Scaling isolated-attosecond-pulse duration by controlling a trajectory parameter

Dian Peng (彭典) ●* and Jean Marcel Ngoko Djiokap ●†

Department of Physics and Astronomy, University of Nebraska, Lincoln, Nebraska 68588-0299, USA

Reaching an ever shorter duration of isolated attosecond pulses (IAPs) is an ongoing mission in attosecond science. Wide usage of long-wavelength driving lasers has greatly broadened bandwidths for generating IAPs. We propose a strategy to further exploit the ability of a long-wavelength laser in producing short IAPs. We introduce a scaling relationship between IAP duration and a trajectory parameter that is associated with the classical cutoff trajectory of high-order harmonic generation (HHG) in gases. This trajectory parameter can facilitate in shortening IAP duration by shaping laser waveform. We demonstrate the effectiveness of our methods with calculations of HHG from Ne by solving the time-dependent Schrödinger equation. A genetic algorithm is used in search for laser parameters. Macroscopic effects in HHG and attopulse generation are investigated. Our results show that increasing laser intensity and using an additional short-wavelength (e.g., deep ultraviolet) laser pulse together with the infrared are effective ways to shorten IAP duration (from 76 to 47 as in our example), for which insightful physical explanations are provided.

I. INTRODUCTION

From nanoseconds (ns) to femtoseconds (fs) and then to attoseconds (as), every breakthrough in achieving shorter light-pulse duration opens up a new era of research and discoveries [1,2]. Attosecond pulses enable us to observe and control electrons in motion on an atomic scale [1–4]. Attosecond pulses have been generated from high-order harmonic generation (HHG) in gases [5–9], optical synthesizing [10], and free-electron lasers [11,12]. They can be either a train of pulses or an isolated single pulse of attosecond duration. The shortest attosecond pulses are isolated attosecond pulses (IAPs) produced from HHG in gases and their duration have been decreasing for over a decade, for example, from 650 as in 2001 [6], to 130 as in 2006 [8], 80 as in 2008 [13], 67 as in 2012 [14], 53 and 43 as in 2017 [15,16]. The characterization of such extreme short duration can be challenging and improvements in attosecond-pulse metrology often accompany records of low duration.

Besides better attosecond-pulse characterization, methods for producing shorter attosecond pulses generally fall into two categories: higher energies and less attochirp. A shorter duration means a wider bandwidth and the central frequency of an attosecond pulse should be at least half of its bandwidth. Thus, to obtain shorter attosecond pulses one wants to produce HHG spectra with higher photon energies. For example, considering a rectangular spectrum (whose bandwidth-duration product of a transform-limited pulse is 3664 eV as), the central

frequency of an 100-as pulse should be at least 18 eV while the central frequency of an 1-as pulse should be at least 1.8 keV. HHG spectra reaching high energies of the water window (282–533 eV) [17–21] or keV region [22,23] are measured, but zeptosecond pulses have not been reported.

The other important aspect in generating short attosecond pulses from HHG in gases is to overcome the attochirp problem. Attochirp is an intrinsic chirp of the HHG process where high-harmonic photons of different frequencies are emitted at different times and consequently attosecond pulses are not transform-limited [8,13,24]. A thin-film filter is commonly used in experiments to compensate the attochirp for a limited frequency range using material dispersion [8,13–16,25]. Special experimental instruments were designed to compress attosecond-pulse duration, for example, with a double-grating compressor [26] or a multilayer XUV mirror [27], whose function bandwidth typically spans tens of electron volts. Attochirp compensation by plasma dispersion has also been investigated theoretically for large photon energies in the water window [28]. Recently, we proposed a novel way of producing transform-limited attosecond pulses for any bandwidth without compensating attochirp by π-phase shifting of frequency stripes in an HHG spectrum [29].

Many studies have contributed to our understanding of the roles that laser-pulse waveform can play in HHG and IAPs [2,3,30–43]. For example, HHG can be enhanced by a linear-ramp shape in the electric field of an optimized laser waveform [41], or by oppositely chirping two pulses for better field alignment [42]. Attochirp can be reduced by confining returning electron trajectories into a short time window [43]. However, few studies reported quantitative descriptions regarding reducing attochirp or shortening IAP duration with laser-pulse shaping. For a one-color pulse, it is known that an averaged attochirp is proportional to the driving laser frequency and thus a longer wavelength is preferred to achieve smaller attochirp [44,45]. Interestingly, in a different

*dpeng3@unl.edu
†marcelngoko@unl.edu

circumstance where pulse shaping is considered we find that an additional *short* wavelength is favored to reduce attochirp and thus shorten IAP duration.

In this paper, we establish a quantitative scaling relationship between IAP duration and a trajectory parameter that is associated with the classical cutoff trajectory of HHG. Specifically, the IAP duration is reported here to be inversely proportional to the trajectory parameter. Upon careful examination of this trajectory parameter, insightful physical interpretations can be drawn regarding reducing attochirp in HHG with pulse shaping. Based on the scaling relationship, strategies of shortening IAP duration with laser-pulse shaping are proposed. We demonstrate the effectiveness of our strategies by performing numerical calculations of HHG from Ne (whose ionization potential is large among rare gases and thus can stand higher laser intensities to achieve larger HHG cutoffs) in both single-atom and macroscopic systems. A genetic algorithm is used in search for laser parameters. Our results show that increasing laser intensity and using an additional short-wavelength (e.g., deep ultraviolet [46–48]) laser pulse together with the infrared can effectively shorten IAP duration in a single-atom system (from 76 to 47 as in our example). Our calculations from focal averaging of a macroscopic system illustrate how variances in driving laser intensities affect outcomes.

We first introduce formulations of the trajectory parameter and discuss its scaling properties in Sec. II. Simulation methods for numerical computation are presented in Sec. III, for both single-atom calculations and three-dimensional intensity averaging in the focal region. The main results are presented in Sec. IV, where we demonstrate how to shorten isolated-attosecond-pulse duration with laser-pulse shaping by controlling the trajectory parameter of HHG. Finally, Sec. V summarizes our results and highlights major conclusions.

II. TRAJECTORY PARAMETER AND ITS SCALING PROPERTIES

An attosecond pulse intensity profile $I(t)$ is generally described as a modulus square of its field amplitude $a(t)$:

$$I(t) \sim |a(t)|^2. \quad (1)$$

The attosecond pulse duration Δt is defined as the full width at half maximum (FWHM) of its intensity profile. Based on an analytical formulation of HHG [36,49], the attosecond-pulse field amplitude generated from a single-cycle HHG spectrum can be approximated as the Fourier transform of an Airy function (see Eq. (21) in [29])

$$a(t) \sim \varepsilon \int_{-\infty}^{\infty} \text{Ai}(x) \text{W}(x) e^{-ixy} dx. \quad (2)$$

Here Ai is the Airy function, which describes the spectral (meaning Fourier-transformed) dipole moment and presents Airy peaks in a single-cycle HHG spectrum [see, e.g., Airy peaks in Fig. 1(b)]. Typically, the analytical HHG formula consists of factors from ionization, propagation, and recombination [36,49]. The Airy function comes from the propagation factor, while ionization and recombination factors are omitted in Eq. (2) for a single-cycle HHG spectrum (ionization factor amounts to an overall constant and recombination factor has much less pronounced variation compared to the oscillating

Airy function) [29]. W is a window function to select HHG frequencies. x and y are scaled dimensionless "energy" and "time," respectively,

$$x = \frac{\hbar\Omega - E_{\text{cut}}}{\varepsilon E_{\text{au}}} - 1.019, \quad y = \frac{E_{\text{au}}}{\hbar}\varepsilon(t - t_r), \quad (3)$$

where $\hbar\Omega$ is the photon energy, E_{cut} is the cutoff energy, $E_{\text{au}} = |e|^2/a_0 = 27.21 \text{ eV}$ (a_0 is the Bohr radius), and the constant 1.019 is related to the maximum of the Airy function. In Eq. (3), ε is the dimensionless trajectory parameter (see Eq. (19) of [29])

$$\varepsilon = \zeta^{1/3}, \quad \zeta = \frac{F(t_r)^2}{2F_{\text{au}}^2}\left[\frac{F(t_r)}{F(t_i)} - \frac{\dot{F}(t_r)}{F(t_r)}(t_r - t_i) - 1\right], \quad (4)$$

where $F(t)$ is the electric field, t_i and t_r are ionization and return times, respectively, of the classical cutoff trajectory, $\dot{F}$ is the time derivative of the electric field, and $F_{\text{au}} = |e|/a_0^2 = 5.142 \text{ GV/cm}$. Note that Eq. (2) works for a single-cycle HHG spectrum, meaning that only one laser cycle should contribute dominantly to the HHG spectrum that is used to generate attosecond pulses [29].

Equation (2) provides a simple generic approximation of attosecond pulses and serves as the foundation of our analyses, from which useful scaling properties of IAPs can be revealed. The Airy function Ai(x) stays the same regardless of driving lasers while information about the driving laser are encoded in scaled variables x and y through parameters E_{cut}, t_r, and ε. For a given W(x), the scaled-time duration Δy is determined. According to Eq. (3), the attosecond-pulse duration Δt is related to Δy in the manner $\Delta t \sim \Delta y/\varepsilon$. Thus, the scaling relationship is that for a given window $W(x)$ the attosecond-pulse duration Δt must be inversely proportional to the trajectory parameter

$$\Delta t \propto 1/\varepsilon. \quad (5)$$

Moreover, from Eq. (2), one sees that a larger value in ε can contribute to a higher intensity of the attosecond pulse. Therefore, we desire a larger trajectory parameter to generate shorter and stronger attosecond pulses.

Based on the structure of trajectory parameter ε given in Eq. (4), one sees a couple of ways to increase its value. First, the F^2 factor in front of the brackets suggests that a higher laser intensity can yield a larger trajectory parameter. Second, the terms inside the brackets are related to the cutoff trajectory and its driving field, suggesting that shaping the laser waveform can enhance ε.

Let us examine terms inside the brackets of Eq. (4). Typically, the electric field strength at the time of ionization is much larger than that at time of return [see, e.g., Fig. 1(a) around times t_i and t_r], meaning that the first term can be ignored [$F(t_r)/F(t_i) \ll 1$]. Next, $(t_r - t_i)$ is the excursion time of the cutoff trajectory and the quantity $\dot{F}(t_r)$ is the slope of electric field at time of return. For a single-color laser field, the excursion time and the slope scale in opposite ways with the driving laser wavelength λ: $(t_r - t_i) \sim \lambda$, while $\dot{F}(t_r) \sim \lambda^{-1}$. Thus, the trajectory parameter ε does not scale with driving laser wavelengths. For example, if we double a wavelength, the trajectory parameter remains the same.
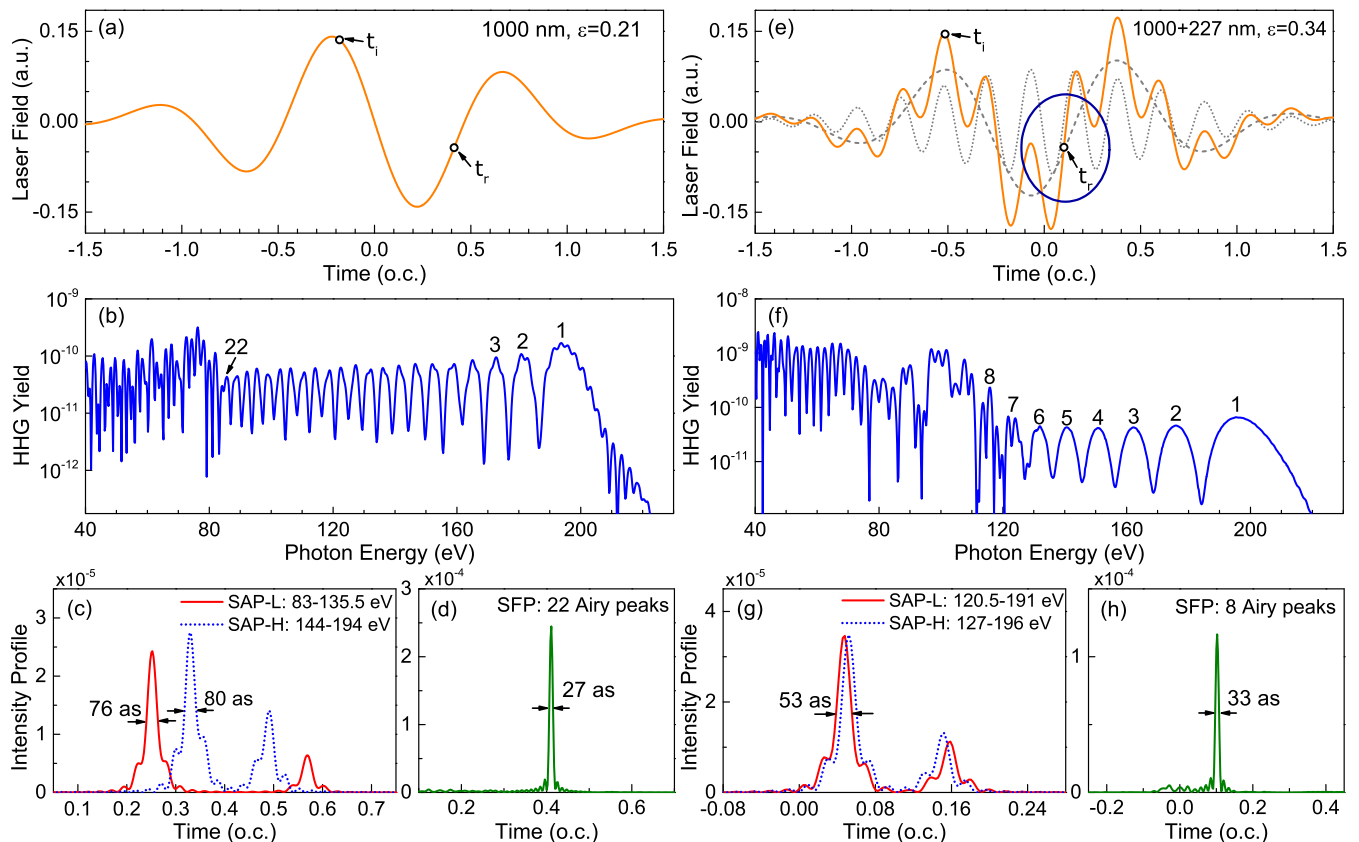
FIG. 1. Enhancing the trajectory parameter by optimizing the laser waveform. (a) The electric field of a one-cycle sine-shaped Gaussian pulse with a carrier wavelength of 1000 nm and a peak intensity of 8×10^{14} W/cm^2. t_i and t_r indicate the ionization and return times of the cutoff trajectory. ε is the trajectory parameter defined in Eq. (4). (b) Calculated HHG spectrum from a Ne atom. Numbers in the figure label Airy peaks. (c) Shortest attosecond pulses from low-frequency (SAP-L, solid red line) or high-frequency (SAP-H, dashed blue line) regions. (d) The striped frequency pulse (SFP) obtained by alternating the phase of neighboring Airy peaks by π. Attopulse duration and bandwidth range are given in (c) and (d). (e)–(h) Same as panels (a) to (d) but for the case of an optimized laser waveform composed with carrier wavelengths of 1000 nm and 227 nm whose electric fields are shown in (e) as dashed and dotted lines, respectively (detailed pulse parameters are listed in Table I for the label "e"). The circle in (e) highlights the steepened electric-field slope at return time due to the additional short wavelength [note that the 1000-nm pulse in (e) has a different CEP from that of (a)].

One way to enhance the trajectory parameter ε is to shape laser-pulse waveform by adding a second pulse, so that both the slope and excursion time obtain large values simultaneously to yield a bigger trajectory parameter. For this purpose, we can start with a *long*-wavelength driving pulse (utilizing its large excursion time) and then add a *short*-wavelength pulse (utilizing its steep slope). With fine-tuning of the pulse waveform by adjusting intensities and relative phases, we can achieve the goal of maximizing ε.

In the following sections, we demonstrate that enhancing the trajectory parameter ε by shaping the laser waveform and increasing the laser intensity is indeed an effective way to shorten the IAP duration.

III. SIMULATION METHODS

A. Single-atom calculation

We calculate HHG spectra produced by a Ne atom interacting with a linearly polarized laser field $F(t)$. Under single-active-electron and electric dipole approximations,

the time-dependent Schrödinger equation (TDSE) of this system is

$$i\frac{\partial}{\partial t}\Psi(\boldsymbol{r}, t) = \left[\frac{\boldsymbol{p}^2}{2} + V(r) + zF(t)\right]\Psi(\boldsymbol{r}, t), \qquad (6)$$

where the laser field is polarized along the z axis and m_e, $|e|$, and $\hbar$ are set to unity in atomic units (a.u.). The atomic potential of Ne is approximated as $V(r) = -(1 + a_1 e^{-a_2 r} + a_3 r e^{-a_4 r} + a_5 e^{-a_6 r})/r$ where parameters a_j $(j = 1\text{–}6)$ are given in Table I of Ref. [50]. TDSE is solved using a time-dependent generalized pseudospectral method [51] in which the wave function is expanded in Legendre polynomials and the time propagation is carried out using a second-order split-operator technique. The convergence of our TDSE calculations was monitored by adjusting the basis size and the grid density in both space and time, where specific parameters are approximately $L \sim 200$ for the maximum angular momentum, $r_{\max} \sim 150$ a.u. for the maximum grid size, $N \sim 3500$ for the number of radial grid points, and the time step ~ 0.075 a.u.

The dimensionless HHG spectrum $S(\Omega)$ is obtained from the Fourier-transformed dipole acceleration along the z axis

$$S(\Omega) = \frac{1}{c^3} \left| \frac{1}{\sqrt{2\pi}} \int_{-\infty}^{\infty} \ddot{D}_z(t) e^{i\Omega t} dt \right|^2, \qquad (7)$$

where c is the speed of light and the time-dependent dipole acceleration $\ddot{D}_z(t)$ is [52]

$$\ddot{D}_z(t) \equiv \langle \Psi(\boldsymbol{r}, t)| - \ddot{z} |\Psi(\boldsymbol{r}, t)\rangle$$
$$= \langle \Psi(\boldsymbol{r}, t)| \frac{\partial V(r)}{\partial z} |\Psi(\boldsymbol{r}, t)\rangle + F(t). \qquad (8)$$

Attosecond pulses are generated by spectrally filtering HHG spectra. Specifically, the attosecond pulse intensity profile $I(t)$ is obtained as the modulus square of its field amplitude

$$I(t) = I_0 \left| \frac{1}{\sqrt{2\pi}} \int_{-\infty}^{\infty} \ddot{D}_z(\Omega) w(\Omega) e^{-i\Omega t} d\Omega \right|^2. \qquad (9)$$

Here I_0 is set to unity, $w(\Omega)$ is a rectangular window function to select HHG frequencies and $\ddot{D}_z(\Omega)$ is the Fourier-transformed dipole acceleration, i.e., $\ddot{D}_z(\Omega) = \frac{1}{\sqrt{2\pi}} \int_{-\infty}^{\infty} \ddot{D}_z(t) e^{i\Omega t} dt$. The attosecond pulse duration Δt is defined as the FWHM of its intensity profile $I(t)$.

B. Three-dimensional focal averaging

To investigate the macroscopic effects of HHG, we employ a three-dimensional (3D) focal averaging model [29], which consists of a one-dimensional (1D) *coherent* intensity averaging along the driving laser propagating axis [53] and a two-dimensional (2D) *incoherent* intensity averaging perpendicular to the axis [54].

The typical geometry of a laser-medium interacting zone for experimental HHG in a gas chamber is a long narrow cylinder. The length of the cylinder corresponds to the width of a gas nozzle and is in the order of millimeters, while the cross-section diameter of the cylinder corresponds to the driving laser beam waist and is in the order of micrometers. The key idea of our 3D focal averaging model is to divide the interacting zone into a bunch of long narrow tubes, where coherence inside tubes is considered with good phase matching in the forward direction and coherent intensity averaging is performed, but coherence between tubes is ignored and incoherent intensity averaging is performed. We test the plausibility of this model by comparing the results between our volume-averaging calculation and Ref. [55] where full 3D propagation is considered, and we see good qualitative agreements for an ionization level of about 11%. This model is expected to work well for a gently focused laser beam where the coherence between tubes can be ignored. We also consider a dilute gas with low ionization so that absorption of high-harmonic radiation and distortion of the driving pulse can be ignored [54].

HHG spectrum with 3D focal averaging is obtained by integrating HHG intensities over the cross section at the medium exit

$$S_{3D}(\Omega) = \int_0^{\rho_{max}} \frac{1}{c^3} |\ddot{D}_{1D}(\Omega, \rho)|^2 2\pi \rho d\rho, \qquad (10)$$

where ρ is the radius of the cross section. $\ddot{D}_{1D}$ is evaluated by coherently summing single-atom HHG amplitudes along the laser propagating axis x for a given ρ:

$$\ddot{D}_{1D}(\Omega, \rho) = \int \ddot{D}_z(\Omega, \rho, x) dx, \qquad (11)$$

where $\ddot{D}_z(\Omega, \rho, x)$ is the Fourier-transformed dipole acceleration for a given laser intensity, as described in Sec. III A.

Attosecond pulses are obtained by integrating intensities over the cross section at the medium exit

$$I_{3D}(t) = \int_0^{\rho_{max}} I_{1D}(t, \rho) 2\pi \rho d\rho, \qquad (12)$$

where I_{1D} is

$$I_{1D}(t, \rho) = \left| \frac{1}{\sqrt{2\pi}} \int_{-\infty}^{\infty} \ddot{D}_{1D}(\Omega, \rho) w(\Omega) e^{-i\Omega t} d\Omega \right|^2. \qquad (13)$$

We assume the gas density is uniform and has dropped its contribution in above integrals.

IV. RESULTS AND DISCUSSION

As outlined in Sec. II, to shorten IAP duration, we want to maximize the trajectory parameter ε. In this section, we demonstrate two ways to enhance the trajectory parameter and how they affect IAPs.

A. Enhancing trajectory parameter by optimizing laser waveform

As a control case, we start with a short Gaussian pulse with a long wavelength. The advantage of using a long wavelength is threefold: it produces a broad bandwidth with large cutoff, presents a smaller averaged attochirp [44,45], and has the potential of yielding a large trajectory parameter, all of which are beneficial to generate short IAPs. To shape the laser waveform, we add a second pulse while keeping the total intensity unchanged. The electric field of the laser pulse is obtained from the time derivative of its vector potential: $F(t) = -dA(t)/dt$ and $A(t)$ is formulated as

$$A(t) = \sum_i -\frac{F_i}{\omega_i} \exp\left(-\frac{2\ln 2}{\tau_i^2} t^2 \right) \sin(\omega_i t + \phi_i), \qquad (14)$$

where F_i is the electric field amplitude, ω_i is the carrier frequency, ϕ_i is the carrier-envelope phase (CEP), and τ_i is the FWHM duration of the ith laser pulse.

For the one-pulse control case, $i = 1$. Specifically, the laser peak intensity is 8×10^{14} W/cm^2 ($F_1 = 0.151$ a.u.), the carrier wavelength is 1000 nm ($= 2\pi c/\omega_1$), $\phi_1 = 0.5\pi$ for a sine shape, and $\tau_1 = 3.3$ fs ($2\pi/\omega_1$) for a single cycle. The electric field $F(t)$ and produced HHG spectrum $S(\Omega)$ are plotted in Figs. 1(a) and 1(b), respectively. Ionization and return times of the cutoff trajectory are labeled in Fig. 1(a) and the corresponding trajectory parameter is $\varepsilon = 0.21$. The HHG spectrum has a wide plateau with $E_{cut} = 194$ eV whose bandwidth covers from about 80 to 200 eV that contains 22 Airy peaks. Airy peaks, which can be approximated by squaring an Airy function, result from subcycle interference of short and long trajectories and appear when a single laser cycle contributes to the HHG spectrum [29,49].

TABLE I. Corresponding data for Fig. 3, including laser-pulse parameters (carrier wavelength λ_i, laser peak intensity I_i and CEP ϕ_i, where i is 1 or 2), trajectory parameter ε, effective Keldysh parameter $\tilde{\gamma}$, and attosecond-pulse duration Δt. The mark $''$ means that the data repeat above.

Label in Fig. 3	Wavelength (nm)		Intensity (10^{14} W/cm²), F_i (a.u.)		CEP (π)				Δt (as)	
	λ_1	λ_2	I_1 (F_1)	I_2 (F_2)	ϕ_1	ϕ_2	ε	$\tilde{\gamma}$	SAP-L	SAP-H
a	1000		8.0 (0.151)		0.5		0.209	0.34	76.2	79.8
b	1000		10.0 (0.169)		0.5		0.226	0.30	68.9	74.4
c	1000	380	5.7(0.127)	2.3(0.081)	1.13	0.69	0.307	1.0	54.4	58.1
d	1000 × 1.2	380 × 1.2	$''$	$''$	$''$	$''$	0.308	0.85	50.8	54.4
e	1000	227	5.3(0.123)	2.7(0.087)	1.15	0.62	0.340	1.7	52.6	52.6
f	1000 × 1.4	227 × 1.4	$''$	$''$	$''$	$''$	0.340	1.2	45.4	49.0
g	1000	227	6.7(0.138)	3.3(0.097)	$''$	$''$	0.366	1.6	47.2	47.2
h	1000 × 1.2	227 × 1.2	$''$	$''$	$''$	$''$	0.370	1.3	43.5	47.2
i	1200	227	4.9(0.118)	3.1(0.094)	1.90	0.38	0.353	2.0	52.6	54.4

We generate a shortest attosecond pulse (SAP) with a conventional filtering of a single spectral range using a procedure described in Ref. [29]. Specifically, an SAP in the low-frequency region (SAP-L) is obtained by scanning spectral bandwidths to find a minimum duration while fixing the lower frequency at the low energy end of the HHG plateau, and an SAP in the high-frequency region (SAP-H) is obtained by scanning spectral bandwidths while fixing the higher frequency at the cutoff. SAPs produced from the HHG spectrum in Fig. 1(b) are plotted in Fig. 1(c). Notice that there are a pair of attosecond pulses and SAP represents the left one emitted at an earlier time that originates from short trajectories (the right one emitted at a later time stems from long trajectories which is excluded in SAP since they do not survive typical phase-matching conditions in HHG [54,56]). SAP-L has a duration of 76.2 as and covers a bandwidth of 83.1–135.5 eV in the low frequency region. SAP-H has a duration of 79.8 as and covers a bandwidth of 144–194 eV in the high frequency region. SAP-H has a longer duration than SAP-L due to larger attochirp in the high frequency region [29].

We previously proposed a method to generate transform-limited IAPs, the striped frequency pulse (SFP), by shifting the phase of every other Airy peak in the HHG spectrum by π [29]. The SFP, plotted in Fig. 1(d), utilizes the entire plateau of 22 Airy peaks (83.1–202.0 eV) and has a duration of 27.2 as. SFP marks the minimum IAP duration one can obtain from the HHG spectrum. We define a ratio of duration between SFP and SAP-L to describe the usability of an HHG spectrum. For example, the usability ratio for the spectrum in Fig. 1(b) is 27/76 = 0.36, showing that a large portion of the HHG spectrum is not used in generating IAPs. This is typically the case when a long driving wavelength is used. Next, we show that by enhancing the trajectory parameter with waveform shaping a broad HHG plateau is less "wasted" in generating short IAPs.

For the two-pulse case, $i = 1, 2$ in Eq. (14). The carrier wavelength of the first pulse is kept at 1000 nm ($= 2\pi c/\omega_1$). An additional pulse can have any wavelength from 200 to 800 nm (the lower bound is close to wavelengths of short deep ultraviolet pulses in experiments [46–48], and the upper bound is smaller than 1000 nm because the trajectory parameter ε does not scale with wavelength). Driving pulse duration

is kept the same as the one-pulse case, i.e., $\tau_1 = \tau_2 = 3.3$ fs. The total intensity of two pulses is set to be 8×10^{14} W/cm² (same as the one-pulse case) and the CEP of each pulse takes a value of $[0, 2\pi]$. There are four independent variables of laser parameters (ω_2, F_1, ϕ_1, and ϕ_2) which are obtained by employing a genetic algorithm (GA) [57] to maximize the trajectory parameter ε. Note that our GA program is fast since it only tries to maximize the trajectory parameter and does not calculate attopulse duration. To guarantee a broad bandwidth for generating short IAPs, we require in our GA program that the high-energy plateau bandwidth in HHG spectrum is at least 50 eV. We carried out multiple runs of GA optimization. The results for each run are not identical but comparable (this is the nature of GA when a large parameter space is searched). Typically, the wavelength of an additional pulse is short (close to 200 nm which is the low limit of the search range) with a comparable intensity to the 1000-nm pulse, and the trajectory parameter is around $0.34 \pm 3\%$. We present one case as an example where the additional pulse has a carrier wavelength of 227 nm ($= 2\pi c/\omega_2$, detailed pulse parameters are listed in Table I for the label "e"). Electric fields $F(t)$ of the optimized pulse are plotted in Fig. 1(e). The corresponding trajectory parameter is $\varepsilon = 0.34$, which is about 60% larger than that of the one-pulse case.

HHG spectrum produced from the optimized laser field is plotted in Fig. 1(f). The high-energy plateau with a cutoff of $E_{cut} = 195$ eV spans approximately from 110 to 210 eV that contains eight Airy peaks. The seventh and eighth Airy peaks have subpeaks due to interference from the low-energy plateau [29]. Airy peaks are wider for a larger trajectory parameter [$\Delta\Omega \propto \varepsilon\Delta x$, see Eq. (3)]. Attosecond pulses SAP-L and SAP-H are plotted in Fig. 1(g) whose duration are the same due to mostly overlapping bandwidths. SAP-L has a duration of 52.6 as and covers a bandwidth of 120.5–191.1 eV. This duration is much shorter compared to the one-pulse case and is approximately proportional to $1/\varepsilon$: $52.6/76.2 \approx 0.21/0.34$. The SAPs in Fig. 1(g) also have higher intensities compared to that in Fig. 1(c). The SFP, plotted in Fig. 1(h), utilizes the entire plateau of eight Airy peaks (111.5–212.0 eV) and has a duration of 32.7 as. The ratio of usability in this case is 33/53 = 0.62, which almost doubles that of the one-pulse case showing that IAP duration is closer to the minimum limit provided by HHG spectrum.
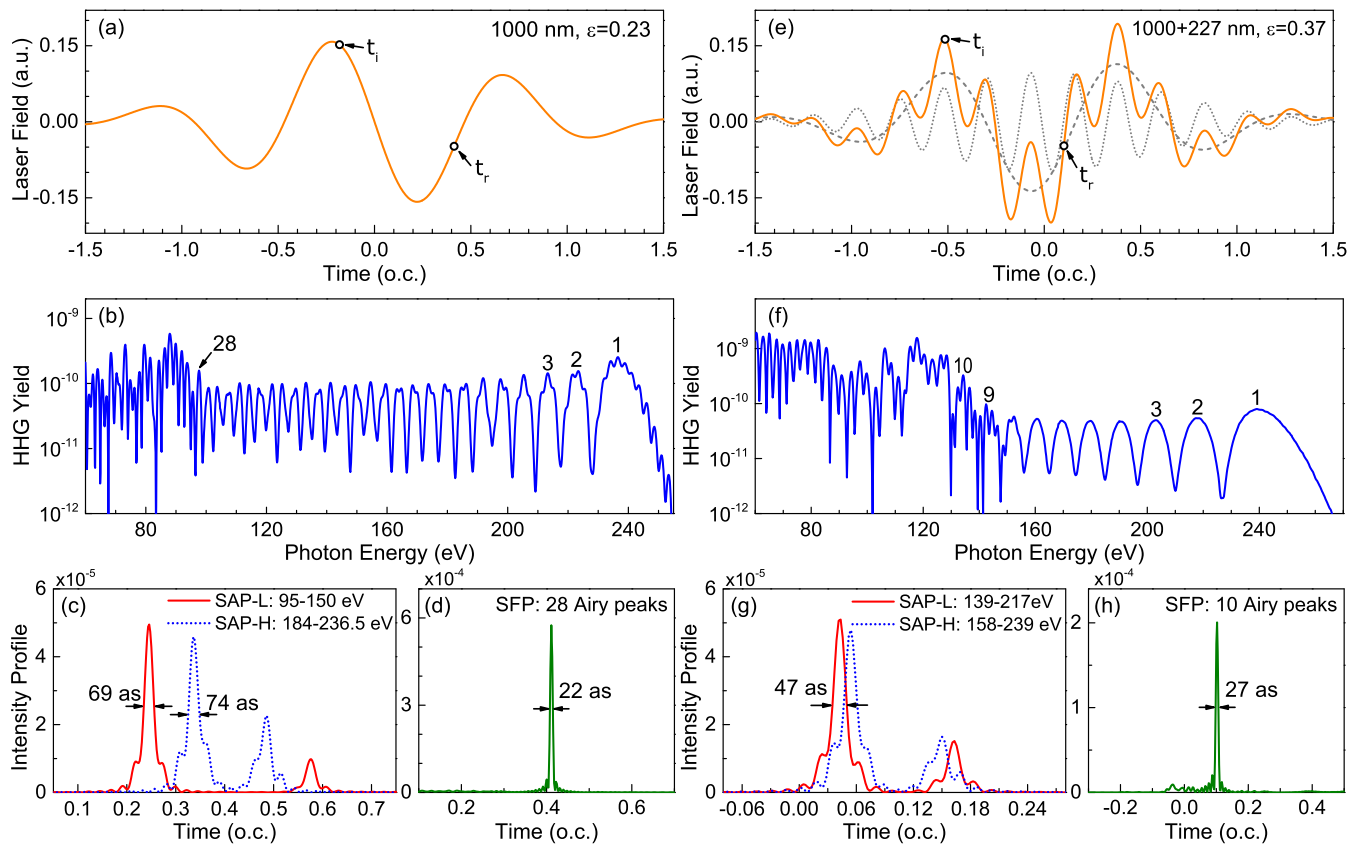
FIG. 2. Enhancing the trajectory parameter by increasing laser intensity. Same as Fig. 1 except that laser intensities are increased from 8×10^{14} W/cm² to 1×10^{15} W/cm².

We see that IAP duration can be shortened significantly with an enhanced trajectory parameter by shaping the waveform of a long-wavelength driving pulse with an additional pulse. GA optimization suggests a short wavelength for the additional laser pulse to maximize the trajectory parameter, which is consistent with our analyses in Sec. II. Let us take a closer look at the electric fields shown in Fig. 1(e). First, the excursion time $(t_r - t_i)$ of the optimized waveform is about the same as that of the one-pulse case (ionizes near peak and returns around zero of 1000-nm field), showing that excursion time is largely determined by the long-wavelength component. At return time t_r, the short wavelength (plotted with a dotted line) combined with the long wavelength (plotted with a dashed line) gives a much steeper slope in the electric field (plotted with a solid line) as compared to that of the long wavelength alone. A steeper slope at return time [i.e., a larger value in $\dot{F}(t_r)$] means that electrons are dragged back within a narrower time window (while energies of returning electrons remain mostly unchanged), which results in less attochirp and shorter attosecond pulses. Therefore, the quantity $\dot{F}(t_r)$ can serve as a meaningful indicator for the amount of attochirp in HHG when performing pulse-waveform shaping.

B. Enhancing trajectory parameter by increasing laser intensity

A second approach to enhance the trajectory parameter ε is to increase laser intensities. To demonstrate how this affects IAPs, we carried out calculations using the same laser param-

eters as that in Fig. 1, except that laser intensities are increased by 25%. For the one-pulse case, the laser peak intensity is 1×10^{15} W/cm² ($F_0 = 0.169$ a.u.) and the trajectory parameter is $\varepsilon = 0.23$. For the two-pulse case, peak intensities are 6.7×10^{14} W/cm² ($F_1 = 0.138$ a.u.) and 3.3×10^{14} W/cm² ($F_2 = 0.097$ a.u.), and the trajectory parameter is $\varepsilon = 0.37$. Electric fields for these two cases with increased amplitudes are plotted in Figs. 2(a) and 2(e). Note that, although the laser intensity is high, the ground state of Ne is not significantly depleted thanks to the very short duration of the pulse (ionization ranges from 5 to 30% for different pulses according to our TDSE estimate by collecting absorbed electron at the grid boundary).

HHG cutoff energy scales linearly with laser intensity [58]. We observe that cutoff energies of HHG spectra shown in Figs. 2(b) and 2(f) increase by approximately 25% compared to lower laser-intensity cases in Fig 1: 236.5 eV (239.0 eV) compared to 193.7 eV (195.4 eV) for the one-pulse (two-pulse) case. The duration of SFP is at the transform-limit level of a plateau bandwidth and thus we expect new SFP duration to decrease by approximately 20% compared to lower laser-intensity cases. For the one-pulse case, the SFP, shown in Fig. 2(d), covers 28 Airy peaks (96.5–249.0 eV) and has a duration of 21.8 as, which decreases 20% compared to 27.2 as. For the two-pulse case, the SFP plotted in Fig. 2(h) covers ten Airy peaks (129.9–256.0 eV) and has a duration of 27.2 as, which decreases 17% compared to 32.7 as.
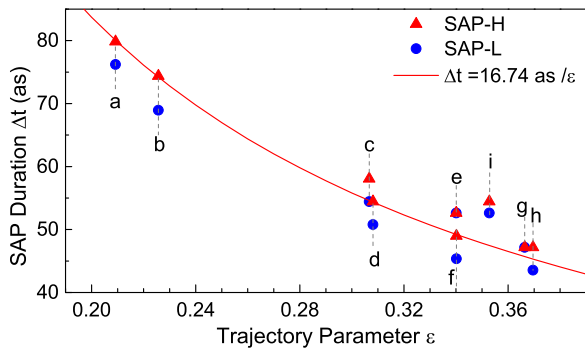
FIG. 3. Scaling of the attopulse duration Δt and trajectory parameter ε. Details of data points with corresponding labels are given in Table I. The line is an estimate of the scaling relationship by averaging points a and b (see text for more explanation).

IAP duration is shortened with an enhanced trajectory parameter ε. For the one-pulse case, SAP-L shown in Fig. 2(c) covers a bandwidth of 94.9–150.3 eV and has a duration of 68.9 as, while SAP-H covers a bandwidth of 183.9–236.5 eV and has a duration of 74.4 as. For the two-pulse case, both SAP-L and SAP-H shown in Fig. 2(g) have a duration of 47.2 as. SAP duration is approximately proportional to $1/\varepsilon$. For example, $69/76 \approx 74/80 \approx 0.21/0.23 \approx 47/53 \approx 0.34/0.37 \approx 0.9$. We also notice that all SAP-H cover about six Airy peaks below the HHG cutoff, i.e., they share the same window $W(x)$ regardless of different frequencies. This can be understood by the approximation in Eq. (2) where attosecond pulses are described as a Fourier transform of the Airy function.

The trajectory parameter ε is enhanced when laser intensity is increased. Looking back at Eq. (4), besides a larger field strength of $F(t_r)$, the slope $\dot{F}(t_r)$ is also larger when laser intensity increases, both of which lead to a larger value in ε. As discussed previously, a bigger slope $\dot{F}(t_r)$ means less attochirp and thus results in shorter IAP duration. This is consistent with previous findings that attochirp (in the middle of HHG plateau) decreases with increased laser intensity [24].

C. Scaling attopulse duration with trajectory parameter

The scaling relationship that the attopulse duration Δt is inversely proportional to the trajectory parameter ε means that the product $\varepsilon \Delta t$ should be a constant. Its value can be estimated by taking an average of the two one-pulse cases and we get $\Delta t = 16.74$ as/ε. Note that here we use SAP-H for Δt since SAP-H is expected to obey the scaling relationship better than SAP-L (as discussed in Sec. II, SAP-H is more likely to have the same window W). The estimated curve is plotted in Fig. 3 together with nine data points from TDSE calculations that are labeled from letter "a" to "i." Detailed data for the nine points are given in Table I with corresponding labels. For example, points a and b are the one-pulse cases for low and high intensities, respectively, while points e and g are optimized two-pulse cases shown previously.

We note that since the analytic formula is based on the assumption that Keldysh parameter is much less than 1 [49], we expect the scaling relationship to work well for pulses with small Keldysh parameters. To better characterize
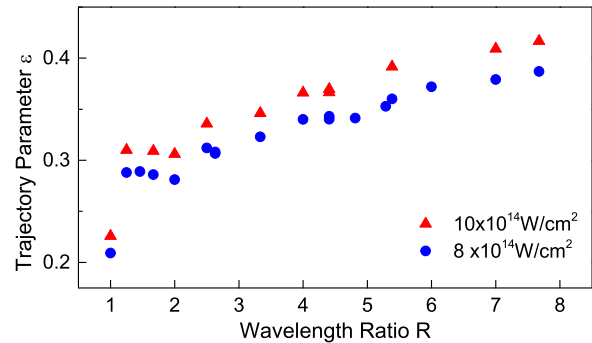

FIG. 4. The trajectory parameter ε for a range of wavelength ratio R ($R = 1$ for single-color cases). Triangles and circles are for high and low laser intensities, respectively.

a shaped pulse, we use an "effective" Keldysh parameter $\widetilde{\gamma}$ (see Eq. (58) of [49])

$$\widetilde{\gamma} \equiv \bar{\omega}\sqrt{2I_p}/F(t_i). \qquad (15)$$

Here I_p is the ionization potential, $F(t_i)$ is the field strength at ionization time, and $\bar{\omega} \equiv max(\omega_1, \omega_2)$, i.e., the max frequency of the two colors [36] which provides an upper bound for the Keldysh parameter. We see from Table I that cases a and b have the smallest $\widetilde{\gamma}$, and this is why we use them to estimate the scaling relationship.

We see in Fig. 3 that points c to h follow the estimated line very well and their effective Keldysh parameters range from 0.85 to 1.7 (noticing that $\widetilde{\gamma}$ does not need to be strictly less than 1 [36]). The laser parameters for point c are also obtained from the GA program except that the wavelength of the second pulse is fixed at 380 nm (we choose this wavelength so that $\widetilde{\gamma} \approx 1$). Points c and e are a bit above the estimated line, meaning that attopulse duration Δt is not short enough. This can be due to (1) the plateau bandwidth is not wide enough and/or (2) the effective Keldysh parameter is large. Both issues can be resolved by increasing laser wavelengths and this is how we obtain points d and f, which overlap exactly the estimated line in Fig. 3. Notice that the trajectory parameter for points c and d (or e and f) are about the same regardless changes in wavelengths. Lastly, we obtain point i by running the GA program with fixed wavelengths 1200 and 227 nm so that we get a larger ε compared to point e. One sees that point i does not follow the estimated line when the effective Keldysh parameter is too large ($\widetilde{\gamma} = 2$).

We see that attopulse duration scales very well with the trajectory parameter when the effective Keldysh parameter is not too much greater than 1. Next, we discuss how the trajectory parameter depends on shaped-laser-waveform parameters like wavelengths, intensities, and phases.

As explained in Sec. II, the trajectory parameter ε does not scale with driving laser wavelengths. We introduce a ratio R between the long and short wavelengths. We take the maximum ε obtained from our GA program for a range of R and plot the results in Fig. 4. One sees clearly that a larger wavelength ratio can provide a larger trajectory parameter. This is consistent with our analyses based on Eq. (4) in Sec. II: the long-wavelength component contributes to a large excursion time while the short-wavelength component

contributes to a large slope, and when we combine these two, they work together to yield a large ε. Therefore, to obtain a large trajectory parameter for generating short attopulses, we want a large ratio between long and short wavelengths, such that the long wavelength can provide a broad bandwidth to afford a short attopulse while the short wavelength keeps the effective Keldysh parameter close to 1.

We consider both low and high laser intensities in Fig. 4 and it is clear that the trajectory parameter is larger for higher intensities. This also explains why ε does not decrease when the ratio R is smaller than 2: when two colors have similar wavelengths, their combined field has a large strength. We notice from our GA results (see, e.g., Table I) that the intensities of the component pulses are comparable. This is understandable from the fact that ε does not scale with the wavelength alone. If one component is much more intense than the other (the extreme case is that one component has zero intensity), the trajectory parameter of a two-color pulse is close to that of a single-color pulse which is the same regardless of the actual wavelength (providing the same intensity and phase). Lastly, the phases of component pulses should be adjusted such that the electric fields align at the time of return so that the slope is effectively steepened.

D. Results for focal averaging

To estimate how our proposed strategies work beyond a single-atom system, we investigate the macroscopic effects of HHG by employing a 3D focal averaging model as described in Sec. III B. To avoid redundant results, we only consider the case of waveform shaping with low laser intensities in Sec. IV A, where estimated ionization is up to 5% (17%) for the one-pulse (two-pulse) case. We consider a gently focused Gaussian laser beam. In the cross section, laser intensities decrease as we increase the maximum radius of the cross section ρ_{max} and we carried out calculations for laser intensities down to about 40% of their maximum values (which are the laser intensities for single-atom calculations in Sec. IV A). Laser pulses with even lower intensities do not contribute much to HHG spectra or attopulse generation. In the propagation direction, we consider a 2% drop in laser peak intensities. A convergence test is carried out to ensure proper choice of grid density. Specifically, we use 24 rings in the cross section to cover laser intensities ranging from 8×10^{14} W/cm^2 to 3.4×10^{14} W/cm^2 for the one-pulse (1000 nm) case and 20 rings in the cross section to cover laser intensities ranging from 5.3×10^{14} W/cm^2 to 2.3×10^{14} W/cm^2 (of 1000-nm pulse) for the two-pulse (1000 + 227 nm) case. We use at least nine points in the propagation direction to cover a 2% intensity drop in each ring.

Our results show that the attosecond pulse duration becomes longer after intensity averaging as compared to the single-atom situation. Figure 5 shows SAP duration (SAP in this section refers to SAP-L) for different laser-intensity ranges in the cross section that are used to perform focal averaging (a 2% intensity drop in the propagation direction is kept the same for all calculations). The lowest laser intensity in the cross section is measured as a ratio to the laser peak intensity used in single-atom calculations. For example, the lowest laser intensity starts from 1, meaning that there is
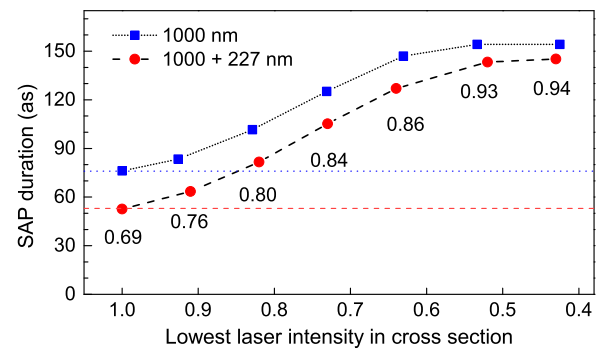

FIG. 5. Shortest attosecond pulse duration with increasing laser intensity range in the cross section. The lowest laser intensity is shown as a ratio to the peak laser intensity that is used in single-atom calculations in Fig. 1. Numbers in figure are ratios of SAP duration between the two-pulse (1000 + 227 nm) and one-pulse (1000 nm) case. Horizontal lines indicate SAP duration from single-atom calculations.

no intensity averaging in the cross section but only in the propagation direction. The horizontal lines in Fig. 5 indicate SAP duration from single-atom calculations. Clearly, except for the very left points, SAP duration with focal averaging for both one-pulse (1000 nm) and two-pulse (1000 + 227 nm) cases are longer than their single-atom levels.

Moreover, as laser-intensity range in the cross section grows (meaning that the lowest laser intensity decreases), SAP duration becomes longer. When the lowest laser intensity is about 0.9, SAP duration is 83.5 as (63.5 as) for the one-pulse (two-pulse) case, which are close to the single-atom level. When the lowest laser intensity is about 0.4, SAP duration is 154 as (145 as) for the one-pulse (two-pulse) case, which are significantly longer than the single-atom level. SAP-duration curve flattens as the lowest laser intensity drops below 50% since lower laser intensities contribute little to HHG spectra.

The ratios of SAP duration between the two- and one-pulse cases are given in Fig. 5 for different lowest laser intensities. One sees that this ratio increases as laser-intensity range grows. For example, when the lowest laser intensity is about 0.9, the ratio is 0.76. But when the lowest laser intensity is about 0.5, the ratio is 0.93, which is much larger than their trajectory-parameter ratio of about 0.6 (0.21/0.34). This means that our proposed scaling relationship (i.e., $\Delta t \propto 1/\varepsilon$) based on single-atom calculations may not work after propagation especially when laser-intensity variance is large. Since our 3D focal averaging is a much-simplified model for the full propagation simulation, further investigations are needed to determine whether and how propagation effects impact our proposed scaling relationship. Nevertheless, our results indicate that to harness the power of the scaling relation and achieve effective reduction in IAP duration one may want to avoid large variance in laser intensities (e.g., use a gently focused laser). As an example, HHG spectra and SAPs are shown in Fig. 6 when the lowest laser intensity is about 0.8 in the cross section (specifically 6.63×10^{14} W/cm^2 for the 1000-nm pulse, and $(4.37 + 2.26) \times 10^{14}$ W/cm^2 for the (1000 + 227)-nm case). One sees that the HHG spectrum
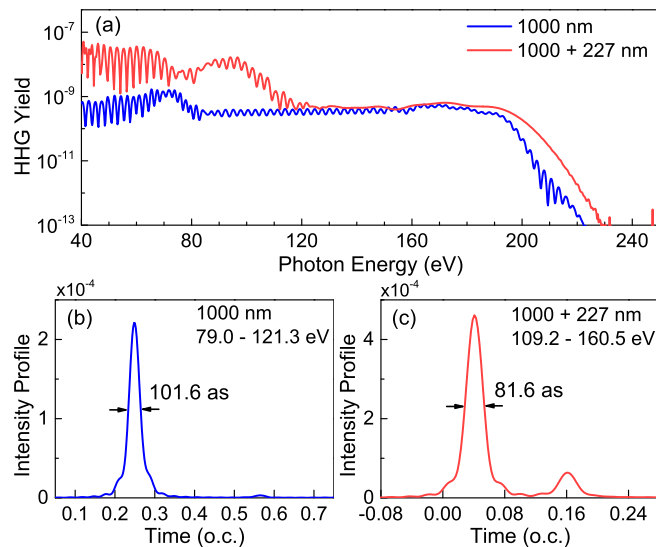
FIG. 6. HHG spectra and SAPs after focal averaging. Top: HHG spectra produced by a single pulse (blue) or two pulses (red). Bottom: Corresponding SAPs from the (b) one-pulse and (c) two-pulse cases. The laser intensity range is such that the peak intensity drops about 20% in the cross section and drops 2% in the propagation direction.

for the two-pulse (1000 + 227 nm) case presents a smooth supercontinuum in the high-energy plateau while the HHG spectrum for the one-pulse (1000 nm) case presents modulated structures. The Airy peaks disappeared in the HHG spectra after focal averaging for both the one-pulse and two-pulse cases. As can be seen from Figs. 4(b) and 4(c), SAP generated from the two-pulse case is about 20% shorter than that from the one-pulse case. One also sees that attosecond pulses coming from long trajectories are much more suppressed after focal averaging compared to single-atom calculations.

V. SUMMARY AND CONCLUSION

Based on analytic analyses and numerical TDSE calculations, we propose a scaling relationship between the isolated-attosecond-pulse duration Δt and a trajectory parameter ε [which is related to the classical cutoff trajectory of HHG and given in Eq. (4)] that the duration is inversely proportional to the parameter: $\Delta t \propto 1/\varepsilon$. This scaling relation tells us that to shorten attopulse duration we want to maximize the trajectory parameter.

Although ε does not scale with the driving wavelength alone, strategies for enhancing the trajectory parameter include (i) increasing laser intensities, and (ii) shaping laser-

pulse waveform by using a two-color pulse where the two component pulses have comparable intensities and large contrasts in wavelengths (i.e., a large wavelength ratio R). We found that the quantity $\dot{F}(t_r)$, i.e., the electric-field slope at return time of the cutoff trajectory, provides useful indication of attochirp in HHG with laser-waveform shaping. It also provides physical interpretations for our strategies of shortening IAP duration by maximizing the trajectory parameter. Specifically, when the laser intensity is increased or a short-wavelength pulse is added to a long-wavelength driver, the slope of the electric field at the return time is steepened, meaning that electrons are dragged back within a narrower time window which yields a smaller attochirp.

With the numerical calculations of HHG from Ne, we demonstrate that the IAP duration indeed can be shortened (from 76 to 47 as in our example) by enhancing the value of the trajectory parameter ε, as long as the plateau bandwidth is sufficiently wide and the effective Keldysh parameter is not too much greater than 1. Note that our proposed scaling relationship and strategies for shortening IAP duration by maximizing the trajectory parameter can apply to various targets. This is because the scaling relationship, derived from Eq. (2), is based on the propagation step of HHG, and the trajectory parameter, given in Eq. (4), only depends on the driving laser pulse. Preliminary results of macroscopic calculations, based on volume intensity averaging in a gas jet, suggest that propagation effects could play an important role. Further investigations may be carried out to consider full propagation effects in various systems (e.g., a hollow waveguide where high gas pressures can be achieved to satisfy phase-matching conditions for long-wavelength drivers [23]).

In conclusion, we propose insightful and quantitative strategies to decrease attochirp in high-order harmonic generation and shorten isolated-attosecond-pulse duration. Our work provides useful guidelines in pulse-waveform shaping regarding generation of short attosecond pulses with long-wavelength drivers.

[1] P. B. Corkum and F. Krausz, Attosecond science, Nat. Phys. **3**, 381 (2007).

[2] F. Krausz and M. Ivanov, Attosecond physics, Rev. Mod. Phys. **81**, 163 (2009).

[3] F. Calegari, G. Sansone, S. Stagira, C. Vozzi, and M. Nisoli, Advances in attosecond science, J. Phys. B: At. Mol. Opt. Phys. **49**, 062001 (2016).

[4] J. Li, J. Lu, A. Chew, S. Han, J. Li, Y. Wu, H. Wang, S. Ghimire, and Z. Chang, Attosecond science based on high harmonic generation from gases and solids, Nat. Commun. **11**, 2748 (2020).

[5] P. M. Paul, E. S. Toma, P. Breger, G. Mullot, F. Auge, P. Balcou, H. G. Muller, and P. Agostini, Observation of a train of attosecond pulses from high harmonic generation., Science **292**, 1689 (2001).

[6] M. Hentschel, R. Kienberger, C. Spielmann, G. A. Reider, N. Milosevic, T. Brabec, P. Corkum, U. Heinzmann, M. Drescher, and F. Krausz, Attosecond metrology, Nature (London) **414**, 509 (2001).

[7] R. Kienberger, E. Goulielmakis, M. Uiberacker, A. Baltuska, V. Yakovlev, F. Bammer, A. Scrinzi, T. Westerwalbesloh, U. Kleineberg, U. Heinzmann, M. Drescher, and F. Krausz, Atomic transient recorder, Nature (London) **427**, 817 (2004).

[8] G. Sansone, E. Benedetti, F. Calegari, C. Vozzi, L. Avaldi, R. Flammini, L. Poletto, P. Villoresi, C. Altucci, R. Velotta, S. Stagira, S. De Silvestri, and M. Nisoli, Isolated single-cycle attosecond pulses., Science **314**, 443 (2006).

[9] Y. Nabekawa, T. Shimizu, T. Okino, K. Furusawa, H. Hasegawa, K. Yamanouchi, and K. Midorikawa, Interferometric autocorrelation of an attosecond pulse train in the single-cycle regime, Phys. Rev. Lett. **97**, 153904 (2006).

[10] M. T. Hassan, T. T. Luu, A. Moulet, O. Raskazovskaya, P. Zhokhov, M. Garg, N. Karpowicz, A. M. Zheltikov, V. Pervak, F. Krausz, and E. Goulielmakis, Optical attosecond pulses and tracking the nonlinear response of bound electrons, Nature (London) **530**, 66 (2016).

[11] P. K. Maroju, C. Grazioli, M. Di Fraia, M. Moioli, D. Ertel, H. Ahmadi, O. Plekan, P. Finetti, E. Allaria, L. Giannessi *et al.*, Attosecond pulse shaping using a seeded free-electron laser, Nature (London) **578**, 386 (2020).

[12] J. Duris, S. Li, T. Driver, E. G. Champenois, J. P. MacArthur, A. A. Lutman, Z. Zhang, P. Rosenberger, J. W. Aldrich *et al.*, Tunable isolated attosecond X-ray pulses with gigawatt peak power from a free-electron laser, Nat. Photon. **14**, 30 (2020).

[13] E. Goulielmakis, M. Schultze, M. Hofstetter, V. S. Yakovlev, J. Gagnon, M. Uiberacker, A. L. Aquila, E. M. Gullikson, D. T. Attwood, R. Kienberger, F. Krausz, and U. Kleineberg, Single-cycle nonlinear optics, Science **320**, 1614 (2008).

[14] K. Zhao, Q. Zhang, M. Chini, Y. Wu, X. Wang, and Z. Chang, Tailoring a 67 attosecond pulse through advantageous phase-mismatch, Opt. Lett. **37**, 3891 (2012).

[15] J. Li, X. Ren, Y. Yin, K. Zhao, A. Chew, Y. Cheng, E. Cunningham, Y. Wang, S. Hu, Y. Wu, M. Chini, and Z. Chang, 53-attosecond X-ray pulses reach the carbon K-edge, Nat. Commun. **8**, 186 (2017).

[16] T. Gaumnitz, A. Jain, Y. Pertot, M. Huppert, I. Jordan, F. Ardana-Lamas, and H. J. Wörner, Streaking of 43-attosecond soft-X-ray pulses generated by a passively CEP-stable mid-infrared driver, Opt. Express **25**, 27506 (2017).

[17] N. Ishii, K. Kaneshima, K. Kitano, T. Kanai, S. Watanabe, and J. Itatani, Carrier-envelope phase-dependent high harmonic generation in the water window using few-cycle infrared pulses, Nat. Commun. **5**, 3331 (2014).

[18] S. L. Cousin, N. Di Palo, B. Buades, S. M. Teichmann, M. Reduzzi, M. Devetta, A. Kheifets, G. Sansone, and J. Biegert, Attosecond streaking in the water window: A new regime of attosecond pulse characterization, Phys. Rev. X **7**, 041030 (2017).

[19] J. Pupeikis, P.-A. Chevreuil, N. Bigler, L. Gallmann, C. R. Phillips, and U. Keller, Water window soft x-ray source enabled by a 25 W few-cycle 2.2 μm OPCPA at 100 kHz, Optica **7**, 168 (2020).

[20] T. Feng, A. Heilmann, M. Bock, L. Ehrentraut, T. Witting, H. Yu, H. Stiel, S. Eisebitt, and M. Schnürer, 27 W 2.1 μm OPCPA

system for coherent soft x-ray generation operating at 10 kHz, Opt. Express **28**, 8724 (2020).

[21] V. E. Leshchenko, B. K. Talbert, Y. H. Lai, S. Li, Y. Tang, S. J. Hageman, G. Smith, P. Agostini, L. F. DiMauro, and C. I. Blaga, High-power few-cycle Cr:ZnSe mid-infrared source for attosecond soft x-ray physics, Optica **7**, 981 (2020).

[22] B. Dromey, S. Kar, C. Bellei, D. C. Carroll, R. J. Clarke, J. S. Green, S. Kneip, K. Markey, S. R. Nagel, P. T. Simpson, L. Willingale, P. McKenna, D. Neely, Z. Najmudin, K. Krushelnick, P. A. Norreys, and M. Zepf, Bright multi-kev harmonic generation from relativistically oscillating plasma surfaces, Phys. Rev. Lett. **99**, 085001 (2007).

[23] T. Popmintchev, M.-C. Chen, D. Popmintchev, P. Arpin, S. Brown, S. Ališauskas, G. Andriukaitis, T. Balčiunas, O. D. Mücke, A. Pugzlys, A. Baltuška, B. Shim, S. E. Schrauth, A. Gaeta, C. Hernández-García, L. Plaja, A. Becker, A. Jaron-Becker, M. M. Murnane, and H. C. Kapteyn, Bright coherent ultrahigh harmonics in the keV X-ray regime from mid-infrared femtosecond lasers, Science **336**, 1287 (2012).

[24] Y. Mairesse, A. de Bohan, L. J. Frasinski, H. Merdji, L. C. Dinu, P. Monchicourt, P. Breger, M. Kovačev, R. Taïeb, B. Carré, H. G. Muller, P. Agostini, and P. Salières, Attosecond synchronization of high-harmonic soft x-rays, Science **302**, 1540 (2003).

[25] K. T. Kim, C. M. Kim, M.-G. Baik, G. Umesh, and C. H. Nam, Single sub$-50-$attosecond pulse generation from chirp-compensated harmonic radiation using material dispersion, Phys. Rev. A **69**, 051805(R) (2004).

[26] M. Mero, F. Frassetto, P. Villoresi, L. Poletto, and K. Varjú, Compression methods for XUV attosecond pulses, Opt. Express **19**, 23420 (2011).

[27] C. Bourassin-Bouchet, Z. Diveki, S. de Rossi, E. English, E. Meltchakov, O. Gobert, D. Guénot, B. Carré, F. Delmotte, P. Salières, and T. Ruchon, Control of the attosecond synchronization of XUV radiation with phase-optimized mirrors, Opt. Express **19**, 3809 (2011).

[28] Z. Chang, Attosecond chirp compensation in water window by plasma dispersion, Opt. Express **26**, 33238 (2018).

[29] D. Peng, A. F. Starace, H. C. Shao, and J. M. N. Djiokap, Minimizing the duration of isolated attosecond pulses, Phys. Rev. A **102**, 063126 (2020).

[30] T. Pfeifer, L. Gallmann, M. J. Abel, D. M. Neumark, and S. R. Leone, Single attosecond pulse generation in the multicycle-driver regime by adding a weak second-harmonic field, Opt. Lett. **31**, 975 (2006).

[31] Z. Zeng, Y. Cheng, X. Song, R. Li, and Z. Xu, Generation of an extreme ultraviolet supercontinuum in a two-color laser field, Phys. Rev. Lett. **98**, 203901 (2007).

[32] P. Lan, P. Lu, W. Cao, Y. Li, and X. Wang, Isolated sub-100-as pulse generation via controlling electron dynamics, Phys. Rev. A **76**, 011402(R) (2007).

[33] B. Kim, J. Ahn, Y. Yu, Y. Cheng, Z. Xu, and D. E. Kim, Optimization of multi-cycle two-color laser fields for the generation of an isolated attosecond pulse, Opt. Express **16**, 10331 (2008).

[34] P. Lan, E. J. Takahashi, and K. Midorikawa, Wavelength scaling of efficient high-order harmonic generation by two-color infrared laser fields, Phys. Rev. A **81**, 061802(R) (2010).

[35] C. Jin, G. Wang, H. Wei, A.-T. Le, and C. D. Lin, Waveforms for optimal sub-keV high-order harmonics with synthesized two- or three-colour laser fields, Nat. Commun. **5**, 4003 (2014).

[36] D. Peng, L.-W. Pi, M. V. Frolov, and A. F. Starace, Enhancing high-order-harmonic generation by time delays between two-color, few-cycle pulses, Phys. Rev. A **95**, 033413 (2017).

[37] B. Xue, Y. Tamaru, Y. Fu, H. Yuan, P. Lan, O. D. Mücke, A. Suda, K. Midorikawa, and E. J. Takahashi, Fully stabilized multi-TW optical waveform synthesizer: Toward gigawatt isolated attosecond pulses, Sci. Adv. **6**, eaay2802 (2020).

[38] D. Greening, B. Weaver, A. J. Pettipher, D. J. Walke, E. W. Larsen, J. P. Marangos, and J. W. G. Tisch, Generation and measurement of isolated attosecond pulses with enhanced flux using a two colour synthesized laser field, Opt. Express **28**, 23329 (2020).

[39] Y. Yang, R. E. Mainz, G. M. Rossi, F. Scheiba, M. A. Silva-Toledo, P. D. Keathley, G. Cirmi, and F. X. Kärtner, Strong-field coherent control of isolated attosecond pulse generation, Nat. Commun. **12**, 6641 (2021).

[40] K. Yang, J.-X. Du, G.-L. Wang, Z.-H. Jiao, S.-F. Zhao, and X.-X. Zhou, Comparative study of different optimization methods for single attosecond pulse generation with a two- or three-color gating scheme, J. Opt. Soc. Am. B **39**, A75 (2022).

[41] S. Haessler, T. Balčiunas, G. Fan, G. Andriukaitis, A. Pugžlys, A. Baltuška, T. Witting, R. Squibb, A. Zaïr, J. W. G. Tisch, J. P. Marangos, and L. E. Chipperfield, Optimization of quantum trajectories driven by strong-field waveforms, Phys. Rev. X **4**, 021028 (2014).

[42] D. Peng, M. V. Frolov, L.-W. Pi, and A. F. Starace, Enhancing high-order harmonic generation by sculpting waveforms with chirp, Phys. Rev. A **97**, 053414 (2018).

[43] I.-L. Liu, P.-C. Li, and S.-I. Chu, Coherent control of the electron quantum paths for the generation of single ultrashort attosecond laser pulse, Phys. Rev. A **84**, 033414 (2011).

[44] J. Tate, T. Auguste, H. G. Muller, P. Salières, P. Agostini, and L. F. DiMauro, Scaling of wave-packet dynamics in an intense midinfrared field, Phys. Rev. Lett. **98**, 013901 (2007).

[45] G. Doumy, J. Wheeler, C. Roedig, R. Chirla, P. Agostini, and L. F. DiMauro, Attosecond synchronization of high-order harmonics from midinfrared drivers, Phys. Rev. Lett. **102**, 093002 (2009).

[46] C. G. Durfee, H. C. Kapteyn, M. M. Murnane, and S. Backus, Intense 8-fs pulse generation in the deep ultraviolet, Opt. Lett. **24**, 697 (1999).

[47] U. Graf, M. Fieß, M. Schultze, R. Kienberger, F. Krausz, E. Goulielmakis, M. Uiberacker, T. Uphues, A. J. Verhoef, V. Yakovlev *et al.*, Intense few-cycle light pulses in the deep ultraviolet, Opt. Express **16**, 18956 (2008).

[48] A. Cartella, A. Trabattoni, D. P. Lopes, E. P. Månsson, F. Frassetto, F. Calegari, F. Légaré, K. Saraswathula, L. Colaizzi, L. Poletto, M. Galli, M. Nisoli, R. M. Vázquez, R. Osellame, S. Stagira, and V. Wanie, Generation of deep ultraviolet sub-2-fs pulses, Opt. Lett. **44**, 1308 (2019).

[49] M. V. Frolov, N. L. Manakov, A. M. Popov, O. V. Tikhonova, E. A. Volkova, A. A. Silaev, N. V. Vvedenskii, and A. F. Starace, Analytic theory of high-order-harmonic generation by an intense few-cycle laser pulse, Phys. Rev. A **85**, 033416 (2012).

[50] X. M. Tong and C. D. Lin, Empirical formula for static field ionization rates of atoms and molecules by lasers in the barrier-suppression regime, J. Phys. B: At. Mol. Opt. Phys. **38**, 2593 (2005).

[51] X.-M. Tong and S.-I. Chu, Theoretical study of multiple high-order harmonic generation by intense ultrashort pulsed laser fields: A new generalized pseudospectral time-dependent method, Chem. Phys. **217**, 119 (1997).

[52] A. D. Bandrauk, S. Chelkowski, D. J. Diestler, J. Manz, and K.-J. Yuan, Quantum simulation of high-order harmonic spectra of the hydrogen atom, Phys. Rev. A **79**, 023403 (2009).

[53] T. Morishita, A. T. Le, Z. Chen, and C. D. Lin, Accurate retrieval of structural information from laser-induced photoelectron and high-order harmonic spectra by few-cycle laser pulses, Phys. Rev. Lett. **100**, 013903 (2008).

[54] P. Antoine, A. L'Huillier, and M. Lewenstein, Attosecond pulse trains using high–order harmonics, Phys. Rev. Lett. **77**, 1234 (1996).

[55] E. Priori, G. Cerullo, M. Nisoli, S. Stagira, S. De Silvestri, P. Villoresi, L. Poletto, P. Ceccherini, C. Altucci, R. Bruzzese, and C. de Lisio, Nonadiabatic three-dimensional model of high-order harmonic generation in the few-optical-cycle regime, Phys. Rev. A **61**, 063801 (2000).

[56] P. Salières, A. L'Huillier, and M. Lewenstein, Coherence Control of High-Order Harmonics, Phys. Rev. Lett. **74**, 3776 (1995).

[57] *Handbook of Evolutionary Computation*, 1st ed., edited by T. Baeck, D. Fogel, and Z. Michalewicz, (CRC Press, Boca Raton, FL, 1997).

[58] J. L. Krause, K. J. Schafer, and K. C. Kulander, High-order harmonic generation from atoms and ions in the high intensity regime, Phys. Rev. Lett. **68**, 3535 (1992).